

# Estimating uncertainty in subsurface glider position using transmissions from fixed acoustic tomography sources

Lora J. Van Uffelen, Eva-Marie Nosal, Bruce M. Howe, Glenn S. Carter, Peter F. Worcester, Matthew A. Dzieciuch, Kevin D. Heaney, Richard L. Campbell, and Patrick S. Cross

Citation: *The Journal of the Acoustical Society of America* **134**, 3260 (2013); doi: 10.1121/1.4818841

View online: <https://doi.org/10.1121/1.4818841>

View Table of Contents: <https://asa.scitation.org/toc/jas/134/4>

Published by the [Acoustical Society of America](#)

---

## ARTICLES YOU MAY BE INTERESTED IN

[The North Pacific Acoustic Laboratory deep-water acoustic propagation experiments in the Philippine Sea](#)  
The Journal of the Acoustical Society of America **134**, 3359 (2013); <https://doi.org/10.1121/1.4818887>

[Observations of sound-speed fluctuations in the western Philippine Sea in the spring of 2009](#)  
The Journal of the Acoustical Society of America **134**, 3185 (2013); <https://doi.org/10.1121/1.4818784>

[Signal processing and tracking of arrivals in ocean acoustic tomography](#)  
The Journal of the Acoustical Society of America **136**, 2512 (2014); <https://doi.org/10.1121/1.4897404>

[Observations of phase and intensity fluctuations for low-frequency, long-range transmissions in the Philippine Sea and comparisons to path-integral theory](#)  
The Journal of the Acoustical Society of America **146**, 567 (2019); <https://doi.org/10.1121/1.5118252>

[Resolution, identification, and stability of broadband acoustic arrivals in Fram Strait](#)  
The Journal of the Acoustical Society of America **141**, 2055 (2017); <https://doi.org/10.1121/1.4978780>

[Source localization in an ocean waveguide using supervised machine learning](#)  
The Journal of the Acoustical Society of America **142**, 1176 (2017); <https://doi.org/10.1121/1.5000165>

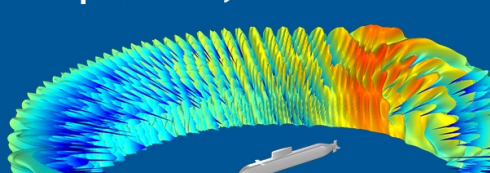
---



**COMSOL Day**  
Acoustics

A free, online event where you can attend multiphysics simulation sessions, ask COMSOL staff your questions, and more

JOIN US MAY 25 »



# Estimating uncertainty in subsurface glider position using transmissions from fixed acoustic tomography sources

Lora J. Van Uffelen,<sup>a)</sup> Eva-Marie Nosal, Bruce M. Howe, and Glenn S. Carter

School of Ocean and Earth Science and Technology, University of Hawaii at Manoa, Honolulu, Hawaii 96822

Peter F. Worcester and Matthew A. Dzieciuch

Scripps Institution of Oceanography, University of California, San Diego, La Jolla, California 92093

Kevin D. Heaney, Richard L. Campbell, and Patrick S. Cross

Ocean Acoustical Services and Instrumentation Systems, Incorporated, Fairfax, Virginia 22039

(Received 8 November 2012; revised 8 April 2013; accepted 9 April 2013)

Four acoustic Seagliders were deployed in the Philippine Sea November 2010 to April 2011 in the vicinity of an acoustic tomography array. The gliders recorded over 2000 broadband transmissions at ranges up to 700 km from moored acoustic sources as they transited between mooring sites. The precision of glider positioning at the time of acoustic reception is important to resolve the fundamental ambiguity between position and sound speed. The Seagliders utilized GPS at the surface and a kinematic model below for positioning. The gliders were typically underwater for about 6.4 h, diving to depths of 1000 m and traveling on average 3.6 km during a dive. Measured acoustic arrival peaks were unambiguously associated with predicted ray arrivals. Statistics of travel-time offsets between received arrivals and acoustic predictions were used to estimate range uncertainty. Range (travel time) uncertainty between the source and the glider position from the kinematic model is estimated to be 639 m (426 ms) rms. Least-squares solutions for glider position estimated from acoustically derived ranges from 5 sources differed by 914 m rms from modeled positions, with estimated uncertainty of 106 m rms in horizontal position. Error analysis included 70 ms rms of uncertainty due to oceanic sound-speed variability. © 2013 Acoustical Society of America. [http://dx.doi.org/10.1121/1.4818841]

PACS number(s): 43.30.Tg, 43.30.Qd [JAC]

Pages: 3260–3271

## I. INTRODUCTION

Gliders equipped with acoustic recording systems can be used in place of more traditional, and more expensive, moorings or ship-suspended receivers to make ocean acoustic measurements. Gliders obtain positioning from GPS at the surface, but less is known about the flight path of the glider during a dive, which can last for several hours. Here, glider acoustic receptions from sources at ranges up to 700 km are used to estimate the uncertainty of modeled underwater glider positions. The ability to determine glider position while it is collecting data underwater will enhance the usefulness of gliders as acoustic sensors, particularly for ocean acoustic tomography applications.

In 1979, 13 acoustic rays were tracked for over 2 months, showing for the first time that acoustic arrivals were resolvable, identifiable, and trackable at a range of 900 km, a fact which surprised researchers just over 30 yr ago (Munk *et al.*, 1995; Spiesberger, 1980). It is these properties of acoustic ray arrivals that enable them to be useful for ocean acoustic tomography. Gliders are in constant motion so receptions on the gliders can not track the stability of a particular ray path; however, since it is known that these arrivals are stable, resolvable ray paths can be identified at many ranges and depths with respect to the acoustic sources.

The Moving Ship Tomography experiment, performed in the summer of 1991 between Bermuda and Puerto Rico, demonstrated the construction of high-resolution maps of ocean temperature using many acoustic receptions at multiple locations around an array of moored sources. A ship deployed a vertical line array (VLA) of receivers at regular intervals as it circumnavigated a 1000-km diameter array consisting of 6 moored acoustic transceivers. At each of the 290 ship stops, made over a period of 51 days, the VLA recorded transmissions from the 6 sources, creating a synthetic array of multiple receivers in the study area. The position of the VLA was determined with a combination of a floating long-baseline acoustic GPS system and an ultra-short baseline system. The position uncertainty of the VLA was about 30 m rms (The AMODE Group, 1994).

The position uncertainty of a glider during a dive is much larger. During a study performed in August–November 2011 off the coast of Oahu, HI, a Seaglider was acoustically tracked using seven acoustic bottom transponders. The positions of the transponders were determined with a shipboard survey. The transponders were interrogated at 9.0 kHz from a transducer suspended from the ship, and each transponder replied at a different frequency ranging from 9.5 to 13.5 kHz. The Seaglider was programmed to record continuously at a sampling frequency of 64 kHz as it operated within the transponder grid, capturing both the interrogation ping as well as each of the transponder replies. The acoustically tracked positions were compared with the glider-estimated positions

<sup>a)</sup>Author to whom correspondence should be addressed. Electronic mail: loravu@hawaii.edu

for two deep (approximately 900 m) dives, Dive 56 and 64. During Dive 56, the glider was tracked on the descent and ascent of the dive, with a departure of approximately 600 m from the predicted position at the deepest part of the dive. The glider was tracked only during the descent of Dive 64, and the tracked and predicted positions differed by approximately 800 m at the termination of the descent.

It is, however, not feasible to use high-frequency acoustic transponders to track a glider during a mission that covers a large geographic area. Narrowband RAFOS signals have been used to position Lagrangian floats (Rossby *et al.*, 1986) and to navigate gliders under ice in the Arctic with travel-time residuals on the order of 2–3 s, which result in positioning uncertainties of a few kilometers (Lee *et al.*, 2010; Sagen *et al.*, 2010). It has been found that exploiting travel-time data from multiple drifting receivers results in improvement of both the sound-speed estimation and localization accuracy (Skarsoulis and Piperakis, 2009). These results were found despite the fact that the narrowband RAFOS signals offer limited time resolution. Broadband signals commonly used in acoustic tomography experiments offer significantly higher travel-time resolution than RAFOS signals, potentially resulting in more precise receiver positioning as well as sound-speed estimation (Howe and Miller, 2004; Duda *et al.*, 2006). These broadband sources can be used to more accurately and precisely locate and navigate gliders or floats while they are underwater and while under ice in polar regions. Such a system is analogous to GPS and has exciting implications for ocean observing systems.

During a brief deployment near Kauai in 2006, a Seaglider equipped with an Acoustic Recorder System (ARS) recorded transmissions from a broadband acoustic source centered at 75 Hz, which had been deployed as part of the Acoustic Thermometry of Ocean Climate (ATOC) experiment. These acoustic receptions verified that acoustic ray arrivals from broadband source transmissions were identifiable in the Seaglider data and that position and velocity estimates were reasonable (Howe and Boyd, 2008).

In April 2010, a pentagonal tomography array consisting of 6 broadband acoustic transceivers and a nearly-full-ocean-depth-spanning Distributed Vertical Line Array (DVLA) was deployed in the Northern Philippine Sea (Fig. 1). Four Seagliders, each equipped with an ARS, were deployed between the fixed transceivers of the array to serve as mobile nodes in the tomography system, theoretically adding 24 acoustic propagation paths for each sequence of acoustic source transmissions. Because the Seagliders are mobile, the resulting paths provide a diverse sampling in range and angular orientation within the study area, i.e., they help fill in Fourier wave number space per the projection-slice theorem (Bracewell, 1956).

One of the primary objectives of the Seaglider aspect of the PhilSea10 Experiment is to determine the accuracy and precision to which the gliders can be located while underwater using swept-frequency signals from moored acoustic tomography sources. With sufficiently small position errors the ambiguity between position and sound speed can be resolved, making the gliders viable receivers for acoustic tomography.

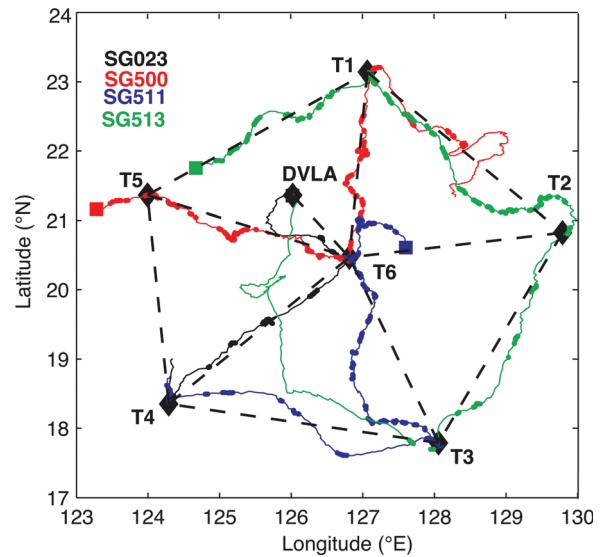


FIG. 1. Acoustic Seaglider tracks in the Philippine Sea. Heavy dots indicate surface positions of gliders while collecting data. Squares indicate deployment positions. Black diamonds indicate positions of the moorings.

Section II outlines the PhilSea10 Experiment. An overview of the data collected on the Seagliders is given in Sec. III. Section IV describes how estimates of range uncertainty were calculated from identifying eigenrays with measured acoustic arrival peaks, and how these estimates of range uncertainty were combined using least-squares to produce estimates of glider position. Results are discussed in Sec. V, and concluding remarks are given in Sec. VI.

## II. PHILSEA10 EXPERIMENT

Much of the recent work in acoustic tomography and long-range propagation has been performed in the somewhat oceanographically benign Northern Pacific Ocean (Worcester and Spindel, 2005). The Philippine Sea offers a much more dynamic environment with high internal wave variability, prominent internal tides, and a complicated system of meso-scale eddies (Colosi *et al.*, 2013).

Broad objectives of the PhilSea10 Experiment are to understand the impact of this oceanographically complex region, inclusive of fronts, eddies, internal waves, internal tides, and spice, on acoustic propagation and, conversely, to use acoustic inversion methods, coupled with ocean models, to yield estimates of the time-evolving ocean state, providing a 4-D sound-speed field for use in acoustic predictions.

The PhilSea10 Experiment spanned a 12-month period from April 2010 to April 2011, enabling a characterization of the oceanographic variability as well as ambient noise throughout the year. Several oceanographic cruises were coordinated in the study region during this time (Worcester *et al.*, 2013).

### A. Moored tomography experiment

The moored tomography array consisted of 6 acoustic transceivers (T1-T6) deployed in a pentagonal arrangement with a radius of approximately 330 km, spanning much of the Northern Philippine Sea (Fig. 1). These subsurface

TABLE I. Transmission characteristics and positions of moored swept-frequency acoustic sources.

Mooring	Transmit Time (s)	Source Delay (ms)	Effective Sweep Time (s)	Frequency (Hz)	Average Source Level (dB re 1 $\mu$ Pa at 1 meter)	Latitude ( $^{\circ}$ N)	Longitude ( $^{\circ}$ E)
T1	0	-8.4	134.977	200-300	184.35	23.13970	127.06792
T2	540	9.6	134.992	140-205	183.82	20.82522	129.78055
T3	1080	57.6	135.033	225-325	181.85	17.78761	128.05815
T4	1620	57.8	135.033	225-325	182.70	18.35123	124.28938
T5	2160	256.0	135.030	205-305	183.97	21.36652	123.98781
T6	2700	-6.0	134.972	200-300	185.75	20.46758	126.81268

moorings each supported a swept-frequency acoustic source (Webb *et al.*, 2002; Morozov and Webb, 2007) with a frequency range of approximately 200–300 Hz, although the frequency characteristics varied from source to source (Table I). The sources were moored at a nominal depth of 1050 m, approximately the depth of the sound channel axis.

The anchor positions of the source moorings were determined by a shipboard survey at the time of deployment (Table I). Since moorings move in response to tidal forcing as well as currents associated with mesoscale eddies, the position of each source was measured once an hour throughout the deployment to within 1.5 m rms using a long-baseline navigation system with an acoustic interrogator on the source and three bottom-mounted acoustic transponders.

The acoustic sources transmitted a linear frequency modulated (LFM) sweep signal for approximately 135 s, every 3 h on odd-numbered yeardays beginning at 0000, 0300, 0600,... 2100 UTC. Although the experiment spanned April 2010 to April 2011, all yeardays have been referenced to 1 January 2010. The sources transmitted sequentially at 540-s intervals. Measured source levels, delay times, and sweep duration varied slightly for each of the moored sources (Table I). Source clock drifts were also measured once per day by comparison with a Rubidium frequency standard with an accuracy of  $\sim$ 1 ms per year.

## B. Acoustic Seaglider experiment

Four Acoustic Seagliders (SG023, SG500, SG511, and SG513) were deployed in November 2010 in various positions around the array; they then transited different paths, roughly clockwise around the array (Fig. 1). The iRobot Seagliders are non-propelled, buoyancy-driven autonomous underwater vehicles (AUVs) (Eriksen *et al.*, 2001). The pitch and roll of the Seagliders are adjusted by shifting an internal mass, and their effective buoyancy is altered by pumping oil between internal and external bladders. Typical horizontal glider speeds for this experiment were on the order of 17 cm/s and vertical descent/ascent rates were approximately 9 cm/s.

After a few initial shallow dives to test ballasting and trim flight parameters, the Seagliders were programmed to dive to their maximum depth of 1000 m. Seabird conductivity and temperature sensors on each glider collected measurements every 10 s above 200 m, every 20 s from 200 to 300 m, and every 40 s below 300 m (Fig. 2). Since the conductivity sensor is not pumped, unfavorable glider orientation (e.g., due to stalling) during a dive sometimes resulted in errors in conductivity measurements.

The Seaglider obtained a GPS position immediately upon surfacing and again immediately prior to diving. During the surface interval, a dive log file was sent to the base station computer via Iridium satellite communication. The temperature and salinity profiles collected during the dive were transmitted as well. The glider pilot had the opportunity to change flight parameters, sampling characteristics, and waypoints of the glider by uploading files to the glider during each surfacing event.

Each glider was equipped with an Acoustic Recorder System (ARS) that collected data from a single hydrophone at a sampling rate of 4 kHz for 3200 s beginning at the nominal transmit time for the T1 source.

The 500-series of Seagliders (SG500, SG511, and SG513) were initially programmed to record every day, including even-numbered, i.e., non-transmission, yeardays to measure ocean ambient noise. On 10 January 2011, however, the schedule was modified to record only on tomography transmission days to conserve battery energy. Based on the projected battery life of the older glider model, SG023 was set to record every fourth day, or every other mooring transmission day.

## III. ACOUSTIC DATA

### A. Acoustic recorder system

The ARS utilized a combination of low-power circuits, power-cycling hardware, and a stable Seascan clock to

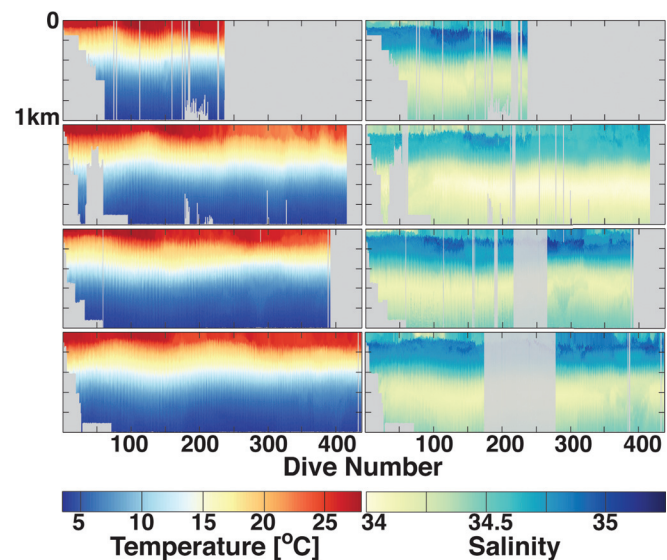


FIG. 2. Temperature (left) and Salinity (right) profiles from SG023, SG500, SG511, and SG513 (top to bottom).

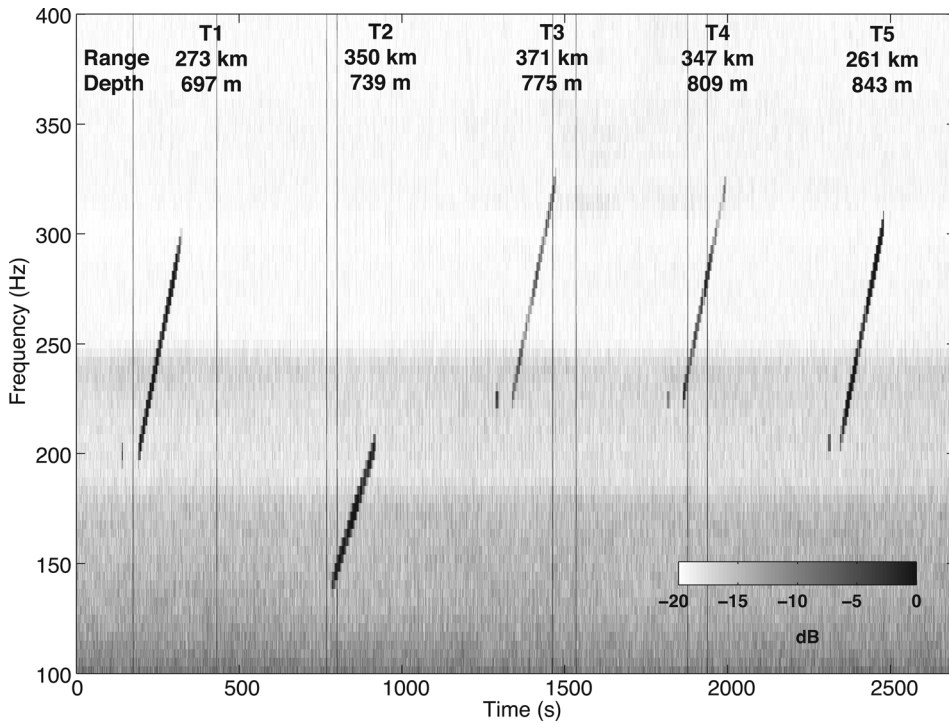


FIG. 3. Spectrogram of data recorded on SG023 During Dive 90 on 1 December 2010 at 0300. Receptions are from moored acoustic sources T1–T5. Source T6 ceased transmitting before the gliders were deployed. The depth of the glider and range to the transmitting source at the time of reception are indicated. Dark vertical streaks in the spectrogram are caused by glider-induced noise.

provide a low-power and versatile acoustic recorder designed to interface with the Seaglider ([Howe et al., 2011](#); [Moore et al., 2007](#)).

The Seascan real-time clock incorporates a temperature-calibrated crystal oscillator, providing a low-power time base with a long-term stability of 1.5 s per year or approximately 1.1 ms per dive. At each surfacing, all the clocks were synchronized to GPS.

GPS was first used to synchronize the glider clock, which then synchronized the ARS system clock, and this then synchronized the Seascan clock. The ARS system clock, which was used to control data acquisition, was synchronized to the Seascan prior to each acquisition, and differences between the Seascan and the ARS system clock were measured immediately prior to and immediately following every 3200-s recording period.

The ARS uses a High-Tech Inc. HTI-92-WB hydrophone to receive the underwater sound. Data were analog filtered between 5 and 1200 Hz, digitized at 4 kHz with a 16-bit analog-to-digital converter, and streamed to a compact flash disk for temporary storage. Data were periodically transferred from the compact flash to a 60 GB power-cycled hard disk for permanent storage either during the apogee phase (transition from descent to ascent) or at the end of the dive.

An ARS log file for each dive was returned via Iridium satellite communication at each glider surfacing. Since it was not feasible to transmit the large acoustic data files via Iridium, the power spectral density for a 16-s segment of recording at the beginning of the acoustic reception was calculated and returned for data quality monitoring. The full acoustic data set stored on the hard drive was retrieved upon glider recovery.

## B. Data processing

Spectrograms were produced for each recording period using a 1024-point FFT and a sliding Hanning window of

length 512 with 50% overlap (Fig. 3). The spectrograms revealed the different frequency characteristics of each source (Table I) and demonstrated high signal-to-noise ratios (SNRs). Short source calibration tones, which immediately preceded the swept-frequency transmissions, were also observable.

Each recording period included receptions from up to 5 sources (T1–T5). The T6 source ceased transmitting before the Seagliders were deployed, so T6 transmissions were not recorded by any of the gliders. Sequences of source transmissions were not recorded for cases in which the glider was at the surface or in the apogee phase of the dive at the nominal transmit time for T1. Recordings were also truncated if the glider surfaced or entered the apogee phase before the end of the 3200-s recording period.

Temporal acoustic arrival structure was obtained using matched filter processing, taking account of the measured effective sweep times and frequencies of the LFM source signals (Table I). Absolute travel-time measurements incorporated source transmission delays and measured source and ARS clock offsets. Offsets of the ARS system clock with respect to Seascan were on average 16.8 ms, with a maximum offset of about 45 ms. These were assumed to be linear drifts during the 3200-s recording period.

Table II summarizes the amount of data collected on the gliders during the PhilSea10 deployment. Because the sequences of source transmissions were spaced by 3 h, and because the

TABLE II. Summary of data collected on Seagliders.

Glider	Dives	T/S Profiles	ARS Files	Source Receptions
SG023	237	452	45	129
SG500	503	832	403	835
SG511	392	782	391	789
SG513	576	876	391	358
Total	1708	2942	1230	2111

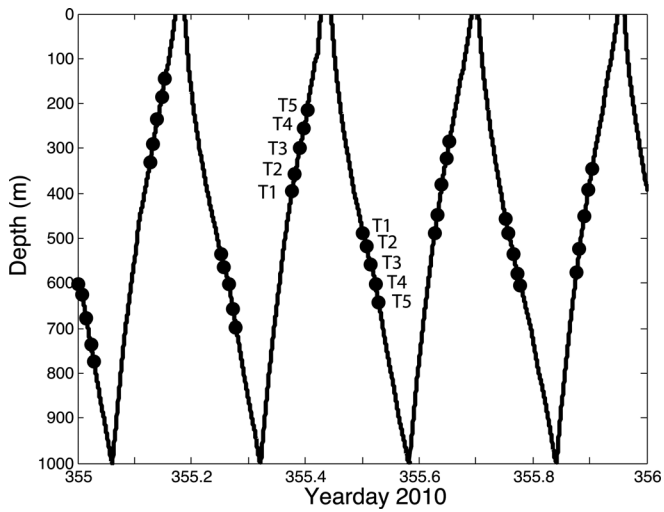


FIG. 4. Glider positions at the time of source receptions superimposed on the dive profile for receptions on SG513 on 2010 Yearday 355.

gliders were often diving for over 6 h at a time, it was common for the gliders to record multiple source transmission sequences during a single dive. Typically this resulted in one recording on the descent of the dive and one on the ascent (Fig. 4).

Because the Seagliders are in continuous motion, the depth and the range at which the glider records the source signals differs from reception to reception (Fig. 5). Recordings were made at depths of up to 1000 m and ranges of up to 700 km. This provides a wide range of propagation paths for acoustic receptions; however, this also makes it impossible to track a particular eigenray arrival peak throughout time since all receptions are independent from one another.

#### IV. QUANTIFYING UNCERTAINTY IN ESTIMATED SEAGLIDER POSITIONS

Disregarding the initial short check-out dives, the average dive time for the gliders was 6.23 h, although dives could

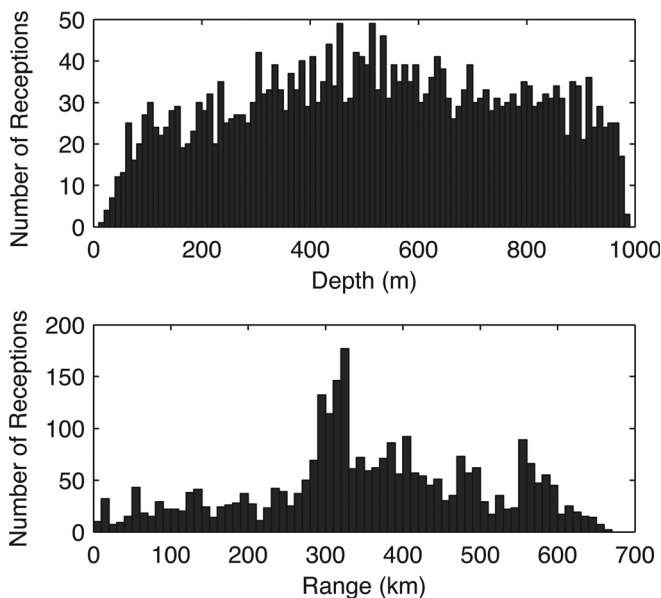


FIG. 5. Spatial distribution of source receptions on Acoustic Seagliders, binned by 10 m in depth (top) and 10 km in range (bottom).

last up to 9 h. The average distance between Seaglider surfacings was 3.55 km, although on a rare occasion, the glider could travel up to 10 km during a single dive.

Although the Seagliders can only obtain GPS fixes during surfacing events between dives, the glider position during a dive is estimated by a kinematic flight model that incorporates the heading and depth of the glider in conjunction with dead-reckoning based on GPS position fixes at the beginning and end of each dive. A Kalman filter uses information on the difference between predicted and actual surfacing locations for navigational control (Eriksen *et al.*, 2001). The estimates of position during a dive were usually smooth trajectories between the GPS surface positions bracketing the dives, but some involved complicated flight paths. This was particularly true for SG500 (Fig. 6), for which difficulties may have been caused by compass errors.

The glider's depth throughout the dive is inferred from a pressure sensor. Because of the physical separation of the hydrophone and the pressure sensor, the accuracy of the reported depth of the hydrophone at the time of reception is dependent on the orientation of the glider at the time of reception and is known to within about a meter.

Rough estimates of the expected acoustic arrival times for each source transmission are obtained using the estimated ranges between the transmitting source and the glider at the time of the reception, assuming a constant sound speed of 1500 m/s. The acoustic arrival times of the maximum peak of each source reception compare well with the Seaglider position-derived result (Fig. 7). On this coarse scale, the tomographic receptions could be used to track the Seagliders as they transited around the moorings during the approximately 100-days deployment period. This comparison also served to point out an obvious clock error for SG511 during 2010 Yeardays 353, 355, and 357 (Fig. 7). The associated receptions were removed from further analysis.

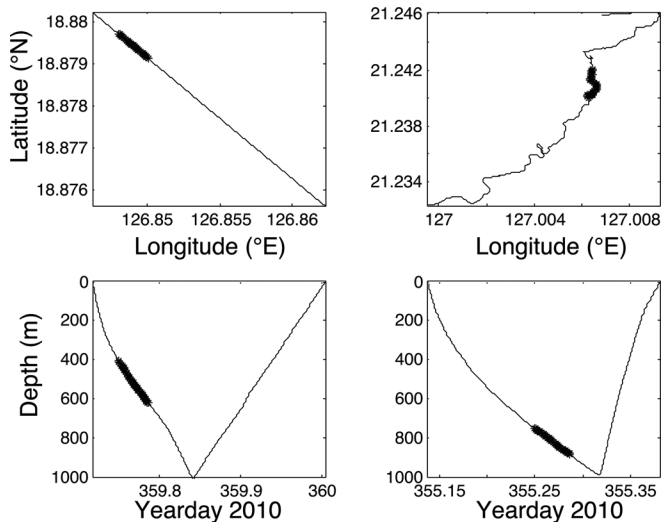


FIG. 6. A typical example of a Seaglider dive (Dive 201 for SG511, left) and a dive whose profile is more erratic (Dive 211 for SG500, right). The upper panels show an overview of the dive track in latitude and longitude, and the lower panels show the dive profile as a function of depth. Highlighted areas in each figure are the times during which the ARS was recording.

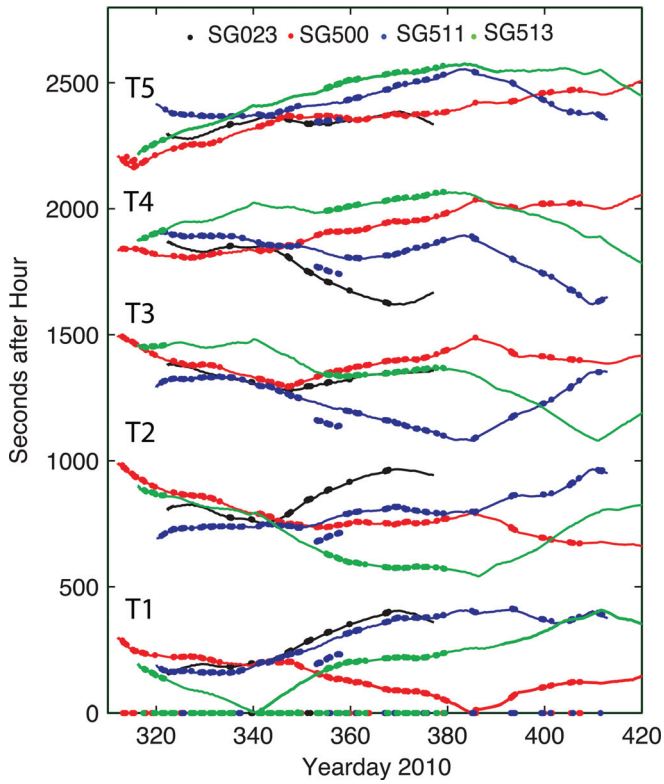


FIG. 7. Dots indicate acoustic arrival times of strongest peak on ARS receivers for SG023, SG500, SG511, and SG513. Solid lines indicate estimated arrival time for a receiver at the surface GPS positions of the respective gliders, assuming a constant sound speed of 1500 m/s. Points on the abscissa indicate receptions for which there were no identified source arrivals either because the source was not transmitting or because the SNR was not adequate. Clock errors of approximately 70 s are evident for SG511 during Yeardays 353–357.

#### A. Sound speed and acoustic propagation modeling

A geometric acoustic ray model was used to predict the acoustic arrival pattern at the estimated glider position at the time of the most intense arrival peak of the reception. The glider was assumed to be stationary during the 135-s recording period.

Time-dependent sound-speed profiles were constructed taking account of measurements collected on all four gliders in the Philippine Sea region throughout the duration of the experiment (Fig. 8). Temperature and salinity profiles were first constructed from the glider temperature and salinity data. Sound speed was then computed using the sound-speed equation of [Del Grosso \(1974\)](#).

The temperature and salinity were first each expressed as time-dependent perturbation fields relative to mean temperature and salinity profiles obtained by taking the average of the World Ocean Atlas monthly profiles from November to March ([Locarnini et al., 2010; Antonov et al., 2010](#)). Gaps in the Seaglider temperature and salinity profiles (Fig. 2) were filled by reconstructing the field using the eigenvectors of the vertical covariances of the temperature and salinity perturbations as a function of depth, i.e., the empirical orthogonal functions (EOFs) of the temperature and salinity, respectively, sorted by time. The lowest 4 EOFs were retained for both the temperature and salinity data,

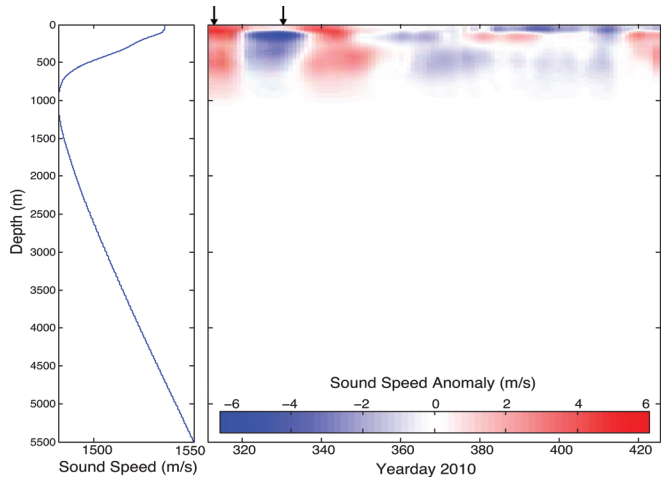


FIG. 8. Time-averaged (left) profile of sound speed and time-dependent (1/day) difference from time-averaged sound-speed profile (right) derived from Seaglider temperature and salinity measurements. Arrows indicate profiles used in the simulations presented in Fig. 10.

accounting for approximately 95% of the variance. The EOFs were tapered smoothly to 0 below 950 m depth using an *e*-folding scale of 500 m to avoid sharp discontinuities in the temperature and salinity fields.

This resulted in a smooth, horizontally averaged, time dependent sound-speed profile.

This estimate of regional sound speed is based on measurements at the four glider positions as these positions changed throughout the deployment. Because of the limited sampling, this profile does not represent changes in the overall sound-speed structure of the entire region but does give an indication of the variability of sound speed in the upper ocean during the experimental deployment.

A single temporally and spatially averaged profile was derived from the time-varying profiles described above. This sound-speed profile was used to obtain acoustic ray trace predictions for the 2111 source/receiver geometries estimated at the time of the Seaglider receptions (Table II).

The earth-flattening transformation was applied to all sound-speed profiles to account for the curvature of the earth along the propagation path prior to inclusion in propagation calculations. The nominal source positions were corrected for the aforementioned mooring motion in *x*, *y*, and *z* throughout the experiment.

#### B. Eigenray identification

Since the Seagliders were in constant motion, each source reception occurred at a different range and depth. As a result, a single eigenray could not be tracked throughout the duration of the experiment as is commonly done in analysis of moored tomographic data. This necessitated eigenray identification for each individual acoustic reception. Despite the lack of statistics at a single depth/range and despite the fact that the acoustic time front pattern was only sampled at one depth rather than by a vertical line array of receivers, in most cases the pattern of multipath arrivals enabled unambiguous eigenray identification.

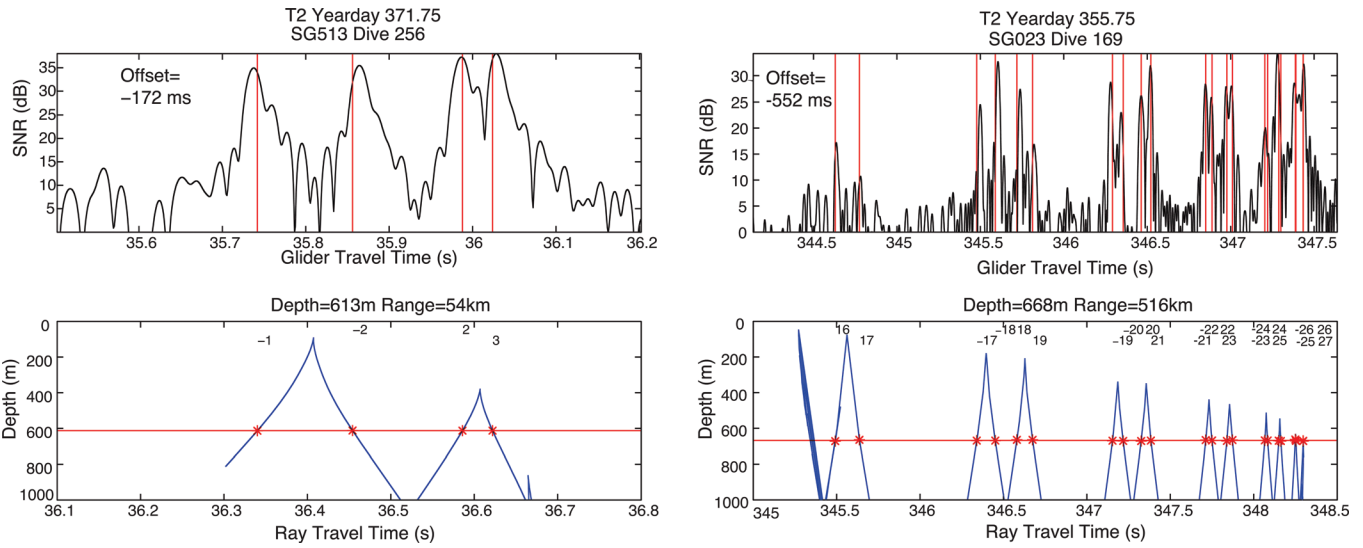


FIG. 9. Received acoustic data (top left) on SG513 from the 1800 UTC transmission of source T2 on 2010 Yearday 371. Vertical lines indicate alignment with predicted eigenrays, and the travel-time offset is indicated on the upper left. Stars mark the intersection of the predicted time front pattern in the upper ocean (bottom left) with a horizontal line indicating the depth of glider at the time of the reception. The Ray ID for these identified eigenrays are indicated on the lower panels. Panels on the left are for a glider recording at a range of 54 km. A much richer pattern of multi-path arrivals is available at greater ranges as shown in the panels on the right for a reception on SG023 from the 1800 UTC transmission of source T2 on 2010 Yearday 355 at a range of 516 km.

Individual peaks in the arrival pattern were matched to the identified eigenrays after adjusting for gross travel-time offsets between the measured and predicted arrival patterns (Fig. 9). These gross offsets were determined visually by shifting the pattern of eigenray arrivals, retaining the inter-ray travel-time separation between eigenrays, to best match the pattern of peaks in the received acoustic data. Adjusting for these gross offsets, eigenray identifications were assigned to associated peaks in the received acoustic data, accounting for small travel-time differences between the predictions, shifted by the gross offsets, and the measured arrivals.

The number of identified eigenrays depends both on the range between the source and the glider and the glider sampling depth. This number varied from few or nil, in receptions that were very shallow and/or at very short range, to

over 20 identifiable eigenrays (Fig. 9, left and right, respectively). Deeper receptions captured more branches of the acoustic time front, resulting in a richer pattern of arrivals. The wide variety of glider acoustic receptions sampled time front branches with acoustic ray identification numbers of just 1 to over 30.

(The sign of the ray identifier  $\pm n$  indicates a positive or negative launch angle at the source and the total number,  $n$ , of ray turning points.)

Because the gliders were diving in the upper 1000 m of the water column, the glider was often shallower than upper cusps of the time front pattern, particularly for the late arriving energy associated with the axial finale. Arrival peaks at times corresponding to the predicted travel times of these cusps are often present (Fig. 10), indicating vertical scattering

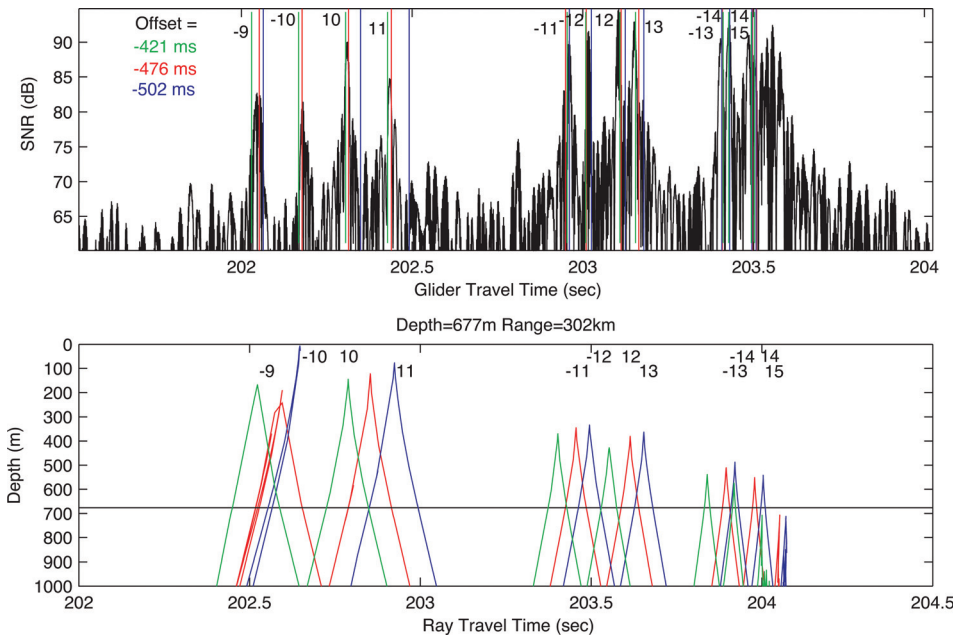


FIG. 10. Acoustic reception and eigenray identification for transmission from T1 on 2010 Yearday 347 at 1200 UTC received on SG500 following the format of Fig. 9. Predictions presented use a mean sound-speed profile (red) as well as selected extreme sound-speed profiles from 2010 Yearday 315 (warm, green) and Yearday 329 (cold, blue). These profiles are indicated by arrows in Fig. 8. Vertical lines in the upper panel show eigenray arrivals shifted in time to match received arrival peaks in colors corresponding with the predictions in the lower panel.

of the time front peaks similar to that seen in the deep ocean (Van Uffelen *et al.*, 2009). These non-geometric arrivals were not directly associated with eigenray peaks in the predictions, but aided in determination of the offsets in the pattern-matching between predicted eigenrays and acoustic data.

To explore the effect of the background sound-speed profile on the predicted acoustic arrival pattern, eigenray predictions for a representative glider reception at a range of 302 km and a depth of 677 m were performed using the mean sound-speed profile as well as two profiles representing the extremes of the measured sound speeds (Fig. 10). Gross offsets between the measured data and the eigenray arrival patterns for each of the predictions were determined independently. Near the axial finale, differences in travel time between the different predictions are very small, but these differences increase for the early eigenrays which correspond to shallow-turning rays with smaller ray IDs. Some early rays that are refracted in the mean and warm profiles, become surface-reflected in the cold profile. These steep ray paths sample the upper ocean where the sound-speed profiles differ most dramatically. The inter-peak offsets of up to 45 ms between the shifted predictions of eigenray travel times and the associated peaks in the acoustic data carry with them information about the ocean sound-speed structure.

The gross offsets between each of the predictions and the acoustic reception ranged from  $-421$  ms for the warmer profile to  $-502$  ms for the colder profile (Fig. 10). This 80 ms difference is for two extreme measurements of ocean sound-speed profiles at a typical range for this experiment, indicating that variability in the background ocean sound speed alone, which represents a horizontal spatial average, can account for up to 80 ms of travel-time uncertainty. The effect on travel time is consistent with the estimate given in Powell *et al.* (2013) of 70 ms rms, which is used in this paper as a representative measure of uncertainty due to oceanic sound-speed variability and is further discussed in Sec. V. Assuming an extreme case for the warmest profile recorded during the experiment, there was still an offset of over 400 ms between the predicted and received arrival times. This travel-time offset is attributed to glider position uncertainty.

### C. Estimate of glider range uncertainty

Eigenray identification is robust, and it has been long observed that offsetting the position of tomographic receivers by a few kilometers does not compromise the eigenray identification (e.g., Gaillard, 1985). Here, gross travel-time offsets between received acoustic arrivals and eigenrays predicted using the mean profile (Fig. 8, left) are used to estimate uncertainty in the range between the source and the glider. A sound speed of 1500 m/s is assumed to convert the gross travel-time offsets to range uncertainties between the transmitting source and the glider.

A compilation of the gross offsets in the arrival pattern for all of the acoustic glider receptions indicated that the uncertainty did not increase as a function of range (Fig. 11, top). If the offsets were due merely to a change in sound speed along a ray path, one would expect that the offset would scale with range. The range offsets between the source and the predicted

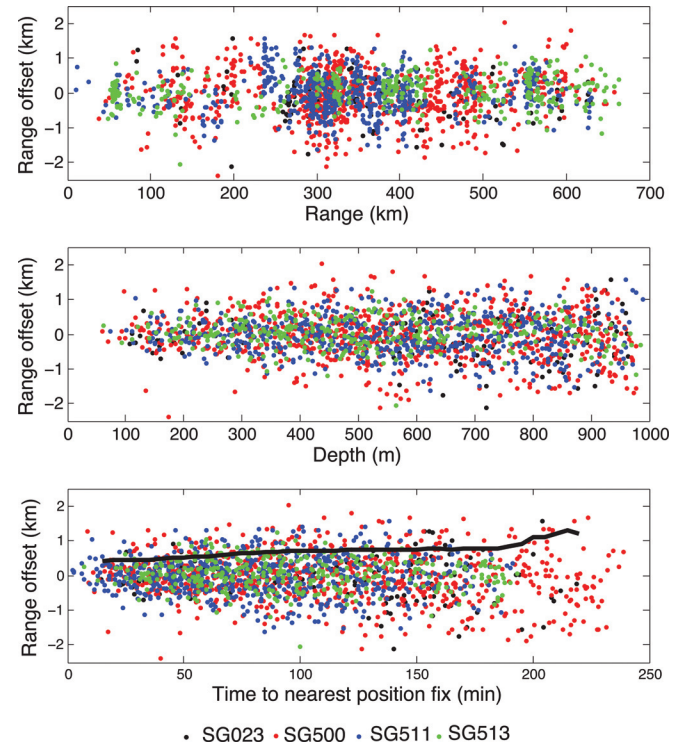


FIG. 11. Gross travel-time offsets between the predicted eigenray arrival pattern and corresponding peaks in measured acoustic data as a function of range (top), depth (middle), and time to nearest GPS fix (bottom). In the bottom panel, the solid line indicates the 75th percentile, calculated by binning the absolute value of the offsets by 30 min at 5 min intervals.

glider position do show a trend with respect to time from the nearest GPS fix, with smaller offsets for receptions near the beginning and end of the dive (Fig. 11, bottom). These offsets increase from 400 m at 15 min from a GPS fix to approximately 1.1 km at 200 min, a typical mid-point of a dive. Because depth in a dive is a proxy for time since a GPS fix, the plot of range offset versus depth (Fig. 11, middle) is similar to the plot of range offset versus time (Fig. 11, bottom).

The range offsets are normally distributed with a mean of  $-18$  m and a standard deviation of 639 m (Fig. 12).

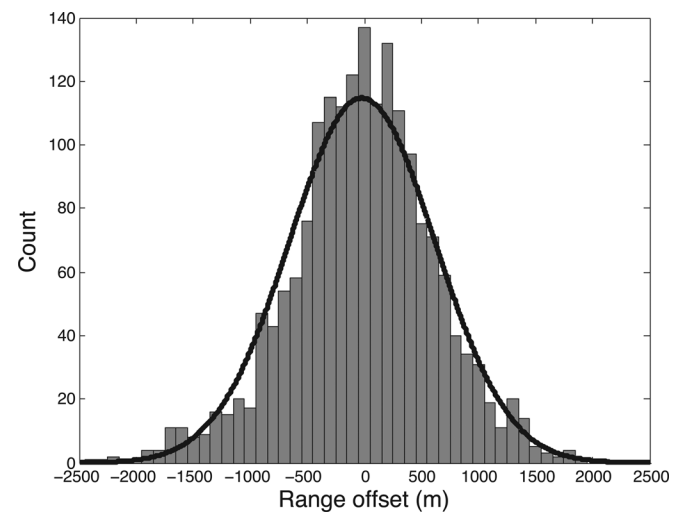


FIG. 12. The distribution of range offset for all acoustic source receptions on all gliders can be fit with a Gaussian curve with a mean of  $-18$  m and a standard deviation of 639 m.

Nearly identical results were obtained from a simple inversion utilizing the same mean sound-speed profile (Fig. 8, left) and the latest-arriving (i.e., most horizontal) identified eigenray from each reception. This inversion allowed for errors of 70 ms rms due to oceanic sound-speed variability, based on ocean model simulations (Powell *et al.*, 2013).

## D. Least-squares localization

Glider range estimates from the acoustic arrival pattern offsets described above were combined for each sequence of five source receptions to obtain a least-squares solution for a single glider position. Because the PhilSea10 acoustic sources did not transmit simultaneously (Table I) and because the gliders are in constant motion, the range estimates are not expected to converge at a single point; however, the least-squares solutions do indicate that the acoustically derived range offsets in a set of sequential source receptions are consistent.

Glider position estimates were calculated using the stochastic inverse method of least squares (Munk *et al.*, 1995) for each of the 270 Seaglider receptions with five source transmissions using the linearized observation equation

$$d = Em + n, \quad (1)$$

where  $d$  is the data vector, consisting of the range offsets for a particular transmission sequence. These range offsets (also called the innovation) were calculated with respect to the glider-estimated position at the time of the reception from T3, the third reception in the sequence. The model vector,  $m$ , represents the  $x$  (east) and  $y$  (north) displacement of the glider relative to the T3 position. The observation matrix,  $E$ , relates the range offsets to the glider position using the source-receiver geometry.

The inverse of  $E$  is denoted by  $B$  and depends on the data error covariance,  $R = \langle nn^T \rangle$ , and the *a priori* model error covariance,  $S = \langle mm^T \rangle$ :

$$B = SE^T(ESE^T + R)^{-1} \quad (2)$$

giving the model estimate  $\hat{m}$  and its associated *a posteriori* model error covariance,  $P$

$$\hat{m} = Bd \quad (3)$$

$$P = (S^{-1} + E^T R^{-1} E)^{-1}. \quad (4)$$

The diagonal terms of  $S$  represent the *a priori* error in the glider position estimate due to the length of time between a surface GPS position fix and the acoustic reception. The average time to a GPS position fix was 100 min and the average glider speed was 17 cm/s and these were used to obtain a measure of glider position error (Table III).

The data covariance matrix,  $R$ , is a combination of measurement and representation errors including:  $r1$ , the uncertainty in range due to eigenray pattern matching, estimated to be  $(10 \text{ ms} \times 1500 \text{ m/s})^2$ ;  $r2$ , the error due to Doppler effects on travel time estimated using the PhilSea10 source signal parameters to be  $(46 \text{ ms} \times 1500 \text{ m/s})^2$  for a glider traveling at 17 cm/s directly toward a source [Duda, 1993, Eq. (16)], a

TABLE III. Statistics of least-squares position estimates and errors.

Data	rms m
$R$ (Data error)	15
$r1$ (Pattern matching)	15
$r2$ (Doppler)	69
$r3$ (Sound speed)	105
$r4$ (Glider motion)	184 (T1 and T5) 92 (T2 and T4) 0 (T3)
Total $R$	223 (T1 and T5) 156 (T2 and T4) 127 (T3)
$d$ (Innovation)	680
Residuals	178
Model	
$S$ ( <i>a priori</i> error)	1020
$P$ ( <i>a posteriori</i> error)	107/105 ( $x/y$ )
$\hat{m}$	914

conservative estimate as the orientation of the glider with respect to the source will vary;  $r3$ , uncertainty due to ocean sound-speed variability estimated to be  $(70 \text{ ms} \times 1500 \text{ m/s})^2$ ; and  $r4$ , the estimated distance between the glider position at the time of the other source receptions relative to the position at the time of the T3 source reception  $[(1080 \text{ s} \times 17 \text{ cm/s})^2$  for T1 and T5,  $(540 \text{ s} \times 17 \text{ cm/s})^2$  for T2 and T4, and 0 for T3].

The least-squares estimated positions differ from the glider-estimated positions at the time of the T3 source reception by 914 m rms with rms offsets of 685 m in  $x$  and 605 m in  $y$  (Fig. 13). The mean of the data residuals is 28 m, and rms is 178 m, consistent with the specified error,  $R$  (Table III).

Error ellipses were calculated from the covariance matrix,  $P$ , indicating the 95% confidence interval (Fig. 13, middle). The error ellipses are near-circular, indicating a sufficient number of paths crossing over a wide range of angles producing a reasonable positioning geometry.

## V. DISCUSSION

This analysis has addressed the uncertainty in the estimated flight path of the glider during a dive cycle, which impacts the precision to which the glider can be positioned at the time of reception. The travel-time offset between data and prediction was used directly to begin to understand the degree of range uncertainty between the source and the predicted glider position. Travel-time offsets between predicted eigenray arrival patterns and acoustic arrivals from moored broadband sources measured on the Seagliders are estimated to be 426 ms rms, which, neglecting all other sources of uncertainty, corresponds to a range error of 639 m rms. Glider position is just one of many factors that contribute to uncertainty in acoustic travel time. Ocean dynamics contribute to travel-time uncertainty, particularly in a highly variable environment such as the Philippine Sea. Results from numerical modeling indicate that sensitivity of rays to inertial-gravity waves, planetary waves, and advection by currents associated with mesoscale eddies can alter ray travel times by as much as 200 ms peak to peak (70 ms rms) (Powell *et al.*, 2013).

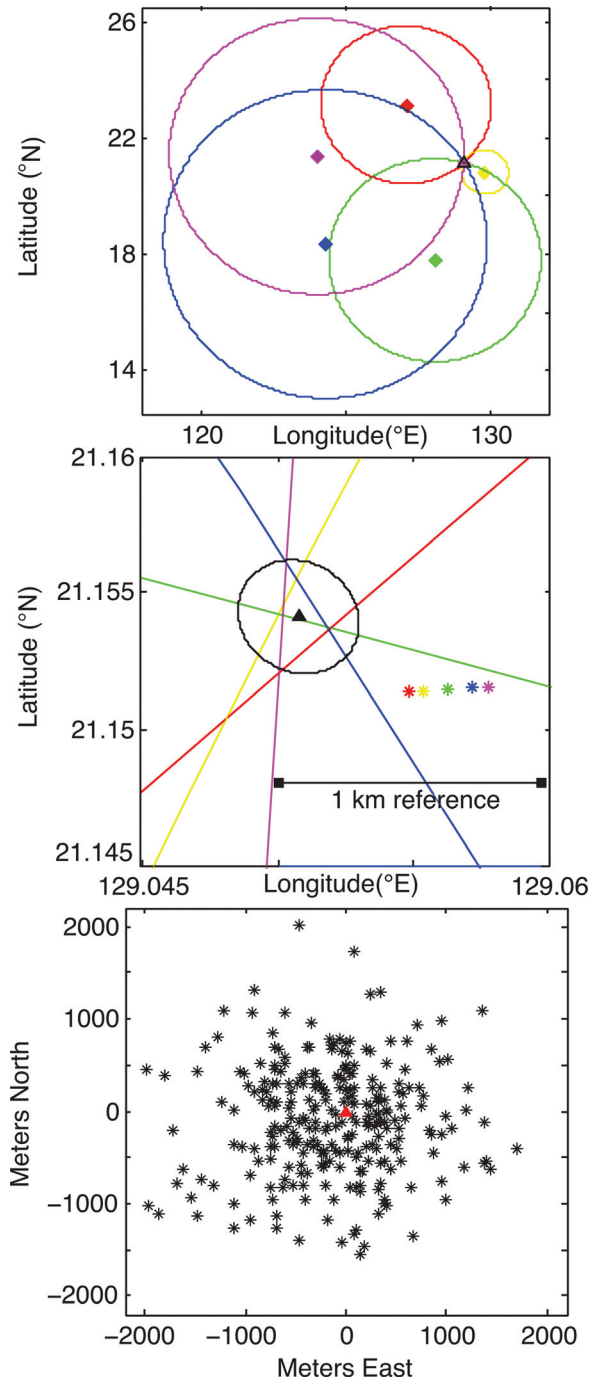


FIG. 13. Acoustically-derived ranges from sources T1 (red), T2 (yellow), T3 (green), T4 (blue), and T5 (magenta) for SG513 Dive 219, Reception 2 (top). Diamonds of the same colors indicate source positions. On this scale, the circles appear to cross at the measured glider location. An expanded view of the region near the intersection of the circle arcs is shown with the glider-estimated positions for each source reception (stars corresponding in color with those listed above) and least-squares estimated position (black triangle), as well as an error ellipse indicating the 95 percent confidence interval (middle). Positions of least-squares solutions for 270 source reception sequences relative to the glider position at the time of the T3 reception, indicated by the red triangle at the origin (bottom).

Internal wave and internal-tide-induced travel-time fluctuations are also a well-recognized source of variability in acoustic travel-time measurements. At typical levels, these fluctuations account for approximately 10 ms rms of travel-

time variability at a range of 1000 km (Cornuelle *et al.*, 1989; Munk *et al.*, 1995). Recent analysis of temperature and salinity data from moored instrumentation deployed as part of the 2009 Pilot Study and Engineering Test performed at the site of the PhilSea10 Experiment indicates that the internal wave mode spectrum, estimated by covariance methods, is similar in shape to the Garrett–Munk (GM) model. The observed internal wave energy, however, is roughly 1.4 times the standard GM level (Colosi *et al.*, 2013). It was also observed that diurnal and semidiurnal internal tides have nearly equal energy compared with the random internal waves.

Relative motion between a moored acoustic source and a Seaglider receiver during an acoustic transmission results in a Doppler shift in the received signal. In a previous experiment conducted off Kauai in 2006, Doppler-derived measurements of glider velocity were determined using receptions of M-sequence signals from an instantaneous broadband source (Howe and Boyd, 2008). Because LFM signals were used in PhilSea10, there is some ambiguity between travel time and Doppler estimates. Doppler effects have not been considered in the acoustic signal processing here; however, Doppler was included as a source of uncertainty in the least-squares position estimation described in Sec. IV D. In future implementations, it would be beneficial to use either instantaneously broadband signals that fully and unambiguously resolve travel time and Doppler or to transmit addition signals such as continuous-wave (CW) tones, from which Doppler can be directly estimated (Duda *et al.*, 2006).

Because the PhilSea10 acoustic sources did not transmit simultaneously (Table I) the glider range errors were evaluated independently; however, these range estimates for each sequence of five source receptions were combined to estimate glider position using the method of least-squares. The offset between the glider-estimated positions at the time of the T3 reception and the positions determined using least-squares is 914 m rms, with estimated uncertainty of about 106 m rms in  $x$  and  $y$ . This offset between glider position and the glider-estimated position is of the same order as that observed during the experiment off the coast of Oahu in which a Seaglider was tracked with acoustic bottom transponders, as described in Sec. I. The rms of the data residuals is much less, 178 m, despite the fact that the acoustically derived range data were separated in time. This consistency in the acoustically derived position suggest that the travel-time offsets described in Sec. IV are largely a result of uncertainty in the glider position. The fact that the acoustically derived range errors were normally distributed also points to positioning errors rather than a constant offset in sound speed. This is further supported by the increase in range error for receptions nearer to the midpoint of a dive, where the glider was farthest removed from a surface GPS fix.

The glider is advected by spatially and temporally varying currents throughout the dive that are unobserved by the single “depth-averaged” current measurements obtained from the offset between the predicted and actual glider positions at the conclusion of the dive. The Philippine Sea is known to be oceanographically energetic, particularly with regards to tidal components. Barotropic tidal currents with

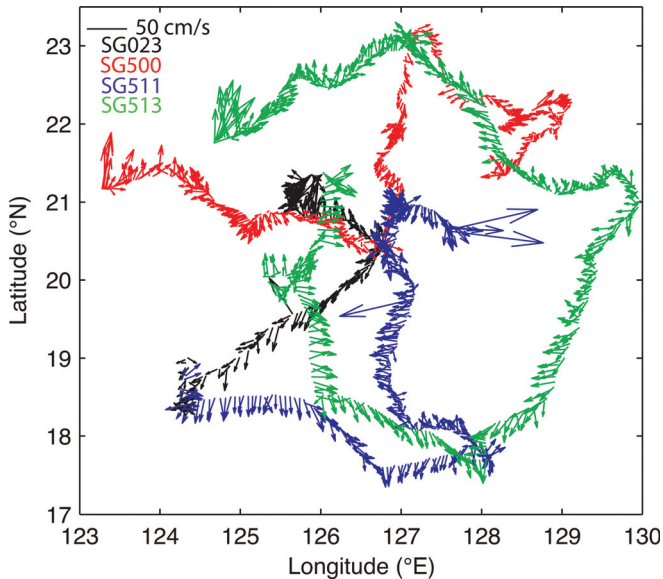


FIG. 14. “Depth-averaged” currents measured by the Seagliders in the Philippine Sea.

temporal scales shorter than a dive and magnitudes of approximately 5 cm/s peak to peak (Egbert and Erofeeva, 2002) could sweep the glider one way and then back again during a 6-h dive. Such motion would be unobserved by the glider’s “depth-averaged” current. Since position/range offsets are observed by the measured acoustic travel-times offsets described here, these offsets can be used to better estimate glider position.

The “depth-averaged” current estimate is not a simple instantaneous vertical average, but a complicated path integral of current as a function of depth, position, and time. Measurements of “depth-averaged” currents from the Seagliders in the Philippine Sea were 18 cm/s rms (Fig. 14). For reference, surface current estimates, based on GPS position differences between surface interval GPS fixes were 42 cm/s rms. Large, near-surface currents could be responsible for the relatively rapid increase in range offset with time to nearest GPS fix (Fig. 11).

## VI. CONCLUDING REMARKS

During the PhilSea10 glider deployment, over 2000 acoustic receptions were recorded at depths up to 1000 m and ranges up to 700 km from five acoustic sources, providing over 2000 cross-sectional snapshots of the oceanographic sound-speed structure of the Philippine Sea. Unambiguous eigenray identification can be made for the majority of acoustic Seaglider receptions, particularly those during which the glider is deep enough to sample many branches of the time front arrival pattern. The fact that individual rays can be resolved and identified implies that the achievable precision of long-range positioning using broadband acoustic sources is ultimately limited by uncertainty in the ocean sound-speed field.

Here gross offsets between received and predicted arrival patterns were utilized to begin to understand the degree of uncertainty in the glider position. This position uncertainty was largely attributed to the presence of water

velocities such as tidal currents which advect the glider during a dive. Because the source transmissions were spaced by 9 min, the gliders moved appreciably between consecutive receptions; therefore, each acoustic reception was considered independently. Despite this, residuals from least-squares estimates of glider position were much smaller than the uncertainty of several kilometers obtained from RAFOS signal localization. The use of simultaneously transmitting sources as well as sources transmitting Doppler-sensitive signals would further improve positioning accuracy.

Moving receiver tomography presents several challenges that do not exist in traditional fixed-geometry tomography experiments, where both source and receiver moorings are precisely navigated and where particular eigenray paths are tracked over time. Because Seagliders are in constant motion, the acoustic time front arrival pattern is sampled at depths that vary from reception to reception. The time front pattern itself is also evolving due to changes in glider range relative to the source, presenting difficulties in obtaining statistics for any particular eigenray path. In addition, the region of the ocean that is sampled varies from one data reception to the next. Simulations have shown that joint inversions for oceanographic properties as well as the position of mobile receivers can be performed (Cornuelle, 1985; Gaillard, 1985; Duda *et al.*, 1995). Future efforts will focus on incorporating ocean velocity models and measurements with acoustic travel-time data to jointly estimate glider position and the ocean sound-speed field. Because statistics at any one range/depth are lacking, this dataset is complementary to the moored tomographic measurements, which provide good statistics from time-series data collected throughout the experiment but represent only a limited number of fixed propagation paths. Ultimately, this dataset will be combined with data from moored instrumentation to enhance tomographic maps of the Philippine Sea region.

## ACKNOWLEDGMENTS

The experiment was funded by the Office of Naval Research Grant N00014-10-1-0334. The PhilSea10 Seaglider dataset was the result of the hard work of many individuals. The authors would especially like to thank Jennie Mowatt, Steve Poulos, Lance Fujieki, Karynne Morgan, Chen-Fen Huang, Captain Chao, Hans Gruber, John Kemp, Barry Ma, and the Captain and crew of the *R/V Roger Revelle*. The authors would also like to acknowledge the Seaglider and ARS technological development and support of Tim Wen, Russ Light, Peter Sabin, and Fritz Stahr at the University of Washington.

- Antonov, J., Seidov, D., Boyer, T., Locarnini, R., Mishonov, A., Garcia, H., Baarmanova, O., Zweng, M., and Johnson, D. (2010). “World Ocean Atlas 2009 Volume 2: Salinity,” in *NOAA Atlas NESDIS 68*, edited by S. Levitus (U.S. Government Printing Office, Washington D.C.), 184 pp.
- Bracewell, R. N. (1956). “Strip integration in radio astronomy,” *Aust. J. Phys.* **9**, 198–217.
- Colosi, J., Van Uffelen, L., Cornuelle, B., Dzieciuch, M., Worcester, P., and Dushaw, B. (2013). “Observations of sound-speed fluctuations in the western Philippine Sea in the spring of 2009,” *J. Acoust. Soc. Am.* **134**, 3185–3200.
- Cornuelle, B., Munk, W., and Worcester, P. (1989). “Ocean acoustic tomography from ships,” *J. Geophys. Res.* **94**, 6232–6250.

- Cornuelle, B. D. (1985). "Simulations of acoustic tomography array performance with untracked or drifting sources and receivers," *J. Geophys. Res.* **90**, 9079–9088.
- Del Gross, V. A. (1974). "New equation for the speed of sound in natural waters," *J. Acoust. Soc. Am.* **56**, 1084–1091.
- Duda, T. (1993). "Analysis of finite-duration wide-band frequency sweep signals for ocean tomography," *IEEE J. Oceanic Eng.* **18**, 87–94.
- Duda, T., Pawlowicz, R., Lynch, J., Cornuelle, B. (1995). "Simulated tomographic reconstruction of ocean features using drifting acoustic receivers and a navigated source," *J. Acoust. Soc. Am.* **98**, 2270–2279.
- Duda, T., Morozov, A., Howe, B., Brown, M., Speer, K., Lazarevich, P., Worcester, P., and Cornuelle, B. (2006). "Evaluation of a long-range joint acoustic navigation/thermometry system," in *Oceans 2006 Conference Proceedings* (IEEE, New York) pp. 1–6.
- Egbert, G., and Erofeeva, S. (2002). "Efficient inverse modeling of barotropic ocean tides," *J. Atmos. Oceanic Technol.* **19**, 183–204.
- Eriksen, C., Osse, T., Light, R., Wen, T., Lehman, T., Sabin, P., Ballard, J., and Chiodi, A. M. (2001). "Seaglider: A long-range autonomous underwater vehicle for oceanographic research," *IEEE J. Oceanic Eng.* **26**, 424–436.
- Gaillard, F. (1985). "Ocean acoustic tomography with moving sources or receivers," *J. Geophys. Res.* **90**, 891–898.
- Howe, B., Van Uffelen, L., Nosal, E., and Carter, G. (2011). "Acoustic Seagliders in PhilSea10: Preliminary results," in *Oceans 2011 Conference Proceedings* (IEEE, New York), pp. 1–8.
- Howe, B. M., and Boyd, M. L. (2008). "Using Seagliders for acoustic receiving and communication," *J. Acoust. Soc. Am.* **123**, 3913.
- Howe, B. M., and Miller, J. H. (2004). "Acoustic sensing for ocean research," *Mar. Technol. Soc. J.* **38**, 144–154.
- Lee, C., Melling, H., Eicken, H., Schlosser, P., Gascard, J. C., Proshutinsky, A., Fahrbach, E., Mauritzen, C., Morison, J., Polyakov, I. (2010). "Autonomous platforms in the arctic observing network," in *Proceedings of the Ocean Obs09: Sustained Ocean Observations and Information for Society Conference* (Venice, Italy), Vol. 2.
- Locarnini, R., Mishonov, A., Antonov, J., Boyer, T., Garcia, H., Baranova, O., Zweng, M., and Johnson, D. (2010). "World Ocean Atlas 2009 Volume 1: Temperature," in *NOAA Atlas NESDIS 68*, edited by S. Levitus (U.S. Government Printing Office, Washington D. C.), 184 pp.
- Moore, S. E., Howe, B. M., Stafford, K. M., and Boyd, M. L. (2007). "Including whale call detection in standard ocean measurements: Applications of acoustic Seagliders," *J. Mar. Technol. Soc.* **41**, 53–57.
- Morozov, A., and Webb, D. (2007). "Underwater tunable organ-pipe sound source," *J. Acoust. Soc. Am.* **122**, 777–785.
- Munk, W., Worcester, P., and Wunsch, C. (1995). *Ocean Acoustic Tomography* (Cambridge University Press, Cambridge, UK), Vol. 149, pp. 259–261, 361–363.
- Powell, B. S., Kerry, C. G., and Cornuelle, B. D. (2013). "Using a numerical model to understand the connection between the ocean and travel-time measurements," *J. Acoust. Soc. Am.* **134**, 3211–3222.
- Rossby, T., Dorson, D., and Fontaine, J. (1986). "The RAFOS system," *J. Atmos. Ocean. Technol.* **3**, 672–679.
- Sagen, H., Sandven, S., Worcester, P., Beszczynska-Moller, A., and Morozov, A. (2010). "The fram strait acoustic system for tomography," in *Proceedings of the "Ocean Obs09: Sustained Ocean Observations and Information for Society" Conference* (Venice, Italy).
- Skarsoulis, E. K., and Piperakis, G. S. (2009). "Use of acoustic navigation signals for simultaneous localization and sound-speed," *J. Acoust. Soc. Am.* **125**, 1384–1393.
- Spiesberger, J. L. (1980). "Stability and identification of ocean acoustic multipaths," *J. Acoust. Soc. Am.* **67**, 2011–2017.
- The AMODE Group (1994). "Moving ship tomography in the North Atlantic," *EOS Trans., Am. Geophys. Union* **75**, 17, 21, 23 (The AMODE Group: Birdsall, T., Boyd, J., Cornuelle, B., Howe, B., Knox, R., Mercer, J., Metzger, K., Spindel, R., and Worcester, P.).
- Van Uffelen, L. J., Worcester, P. F., Dzieciuch, M. A., and Rudnick, D. L. (2009). "The vertical structure of shadow-zone arrivals at long range in the ocean," *J. Acoust. Soc. Am.* **125**, 3569–3588.
- Webb, D., Morozov, A., and Ensign, T. (2002). "A new approach to low frequency wide-band projector design," in *Oceans MTS/IEEE Conference Proceedings*, edited (Biloxi, MS), pp. 2342–2349.
- Worcester, P., Dzieciuch, M., Mercer, J., Andrew, R., Dushaw, B., Baggeroer, A., Heaney, K., D'Spain, G., Colosi, J., Stephen, R., Kemp, J., Howe, B., Van Uffelen, L., and Wage, K. (2013). "The North Pacific Acoustic Laboratory (NPAL) deepwater acoustic propagation experiments in the Philippine Sea," *J. Acoust. Soc. Am.* **134**, 3359–3375.
- Worcester, P. F., and Spindel, R. C. (2005). "North Pacific Acoustic Laboratory," *J. Acoust. Soc. Am.* **117**, 1499–1510.